Title

Tunable Magnetoelastic Effects in Voltage-Controlled Exchange-Coupled Composite Multiferroic Microstructures

Journal

ACS Applied Materials & Interfaces, 12(5)

ISSN

1944-8244

Authors

Xiao, Z
Conte, R Lo
Goiriena-Goikoetxea, M
et al.

Publication Date

2020-02-05

DOI

10.1021/acsami.9b20876

Peer reviewed

Tunable Magnetoelastic Effects in Voltage-Controlled Exchange- Coupled Composite Multiferroic Microstructures

Z. Xiao,[△] R. Lo Conte,[△] M. Goiriena-Goikoetxea, R. V. Chopdekar, C.-H. A. Lambert, X. Li,
A. T. N'Diaye, P. Shafer, S. Tiwari, A. Barra, A. Chavez, K. P. Mohanchandra, G. P. Carman, K. L. Wang,
S. Salahuddin, E. Arenholz, J. Bokor,* and R. N. Candler*

ABSTRACT: The magnetoelectric properties of exchange-coupled Ni/ CoFeB-based composite multiferroic microstructures are investigated. The strength and sign of the magnetoelastic effect are found to be strongly correlated with the ratio between the thicknesses of two magnetostrictive materials. In cases where the thickness ratio deviates significantly from one, the magnetoelastic behavior of the multiferroic microstructures is dominated by the thicker layer, which contributes more strongly to the observed magnetoelastic effect. More symmetric structures with a thickness ratio equal to one show an emergent interfacial behavior which cannot be accounted for simply by summing up the magnetoelastic effects occurring in the two constituent layers. This aspect is clearly visible in the case of ultrathin bilayers, where the exchange coupling drastically affects the magnetic behavior of the Ni layer, making the Ni/CoFeB bilayer a promising next-generation synthetic magnetic system entirely. This study demonstrates the richness and high tunability of composite multiferroic systems based on coupled magnetic bilayers compared to their single magnetic layer counterparts. Furthermore, because of the compatibility of CoFeB with present magnetic tunnel junction-based spintronic technologies, the reported findings are expected to be of great interest for the development of ultralow-power magnetoelectric memory devices.

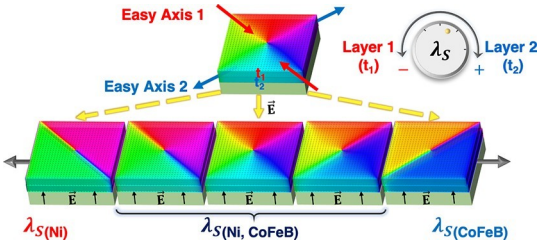

KEYWORDS: *magnetoelastic, multiferroic, voltage-controlled, exchange-coupled, magnetic microstructures, composite films, magnetic properties, magnetic domains, XMCD−PEEM imaging, magnetoelectric*

INTRODUCTION

Magnetoelectric material systems are of great interest for the development of ultralow-power spintronic devices.[1−3] The ability to control magnetization through an electric field offered by such material systems allows for an energy-efficient voltage- based approach to the control of on-chip magnetic nanostruc- tures.[4−7] Accordingly, the development of efficient magneto- electric systems with tunable properties is of great scientific and technological importance.

Magnetoelastic composite multiferroic systems[5,8,9] are among the most promising magnetoelectric systems for spintronic devices. They rely on the combination of piezoelectric and magnetostrictive materials, where the electrically generated strain in the piezoelectric layer is used to reorient the magnetization state of the magnetic layer.[10−13] So far, much work has been done on systems by employing a single magnetostrictive material with efforts focused on finding novel magnetostrictive/piezoelectric heterostructures with large mag- netoelastic coupling.[14−16] However, this approach does not offer much flexibility for tuning the magnetoelastic coupling of a defined system.

In this study, we show that multiferroic systems with a composite magnetic layer can potentially offer much richer magnetoelectric properties with the possibility to tune such

properties by tailoring the magnetic layer composition. Despite its high potential, this avenue has until now remained mostly unexplored.

We report an investigation of the magnetoelectric properties of model composite multiferroic systems consisting of a $[Pb(Mg_{1/3}Nb_{2/3})O_3]_{1-x}-[PbTiO_3]_x$ (PMN−PT)[11] piezoelec- tric substrate and exchange-coupled magnetic Ni/CoFeB bilayers. The magnetoelastic coupling of these systems are studied by observing the electric field-induced magnetic reorientation in Ni/CoFeB microstructures by X-ray magnetic microscopy. The systems show a magnetoelastic effect that depends on the relative thickness of the two magnetic layers, offering a new degree of tunability. Micromagnetic simulations are used to better comprehend the magnetoelastic properties of the investigated systems, unveiling a behavior that cannot be described by simply combining the magnetoelastic responses of the two constituent magnetostrictive materials.

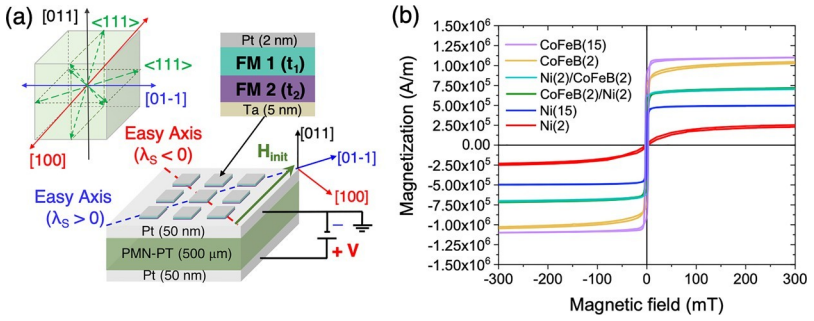

Figure 1. (a) Sample schematic and crystallographic orientation of the PMN−PT crystal with the surface normal along the [011] direction. After patterning, the magnetic microstructures were initialized by an external magnetic field, $\mu_0 H_{init}$ = 300 mT, applied as in the schematic. (b) SQUID magnetometry hysteresis loops for different magnetic thin films, before patterning, on PMN−PT investigated in this study (layer thickness in nm). The magnetic field was applied in-plane along the [01−1] direction.

Experimental Setup and Magnetic Characterization. The material systems of interest consist of Ni/$Co_{40}Fe_{40}B_{20}$ microstructures of different thickness combinations deposited by dc magnetron sputtering on top of 500 μm thick piezoelectric $[Pb(Mg_{1/3}Nb_{2/3})O_3]_{0.69}-[PbTiO_3]_{0.31}$ (PMN−PT) single-crystal substrates with both the top and the bottom surfaces covered using 50 nm thick Pt electrodes. The piezoelectric substrates have the [011] pc (pseudocubic; in the following, this will be omitted for simplicity) crystallographic direction pointing out of the surface plane, as shown in Figure 1a, and are electrically prepoled along this direction with polarization pointing “up” before depositing and patterning the magnetic bilayer on top of it. The Ni/CoFeB microstructures are 2 μm × 2 μm in size. For more details on sample preparation, refer to the work by Xiao et al.[17]

The first hint of the emergent behavior of the investigated multiferroic systems is given by the magnetic properties of Ni/ CoFeB thin films extracted through superconducting quantum interference device (SQUID) magnetometry measurements. The amorphous or nanocrystalline state for the deposited magnetic layers is verified by X-ray diffraction (XRD) (Supporting Information S0). As shown in Figure 1b, single- layer CoFeB thin films (purple and yellow curves in Figure 1b) are found to have the highest saturation magnetization value, M_S ≈ 1.1 × 10^6 A/m, among the investigated samples. On the other hand, samples with a 15 nm thick Ni layer (the blue curve in Figure 1b) show a lower M_S of 5 × 10^5 A/m. The M_S values for the aforementioned thin films are close to the previously reported ones, for CoFeB to be 1 × 10^6 A/m[18] and for Ni to be 4.8 × 10^5 A/m.[19] Finally, bilayer samples having a thickness of 2 nm for both CoFeB and Ni (cyan and green curves in Figure 1b) show an average M_S value of 7.4 × 10^5 A/m, regardless of the stacking order. The shape of the bilayer MH loop combines the features of both the Ni thin film and CoFeB thin film, and both coercivity and saturation magnetization have the intermediate values of the two individual layers. This result suggests the magnetic properties of the bilayer result from the interplay between the two magnetic layers being coupled to each other. Even stronger evidence of the importance of coupling between magnetic layers is given by the hysteresis loop obtained for the Ni(2 nm) sample (the red line in Figure 1b). Compared to 15 nm thick Ni with a square MH loop, the thin Ni(2 nm) loop indicates a superparamagnetic state, as shown by very low saturation magnetization (at the maximum applied magnetic field), together with the absence of any significant remanence (see Figure S1a for more details).[20] This finding is in accordance with a previous study showing superparamagnetism in an

ultrathin Ni film with a thickness down to 2 nm.[21] However, Ni(2 nm)/CoFeB(2 nm) and CoFeB(2 nm)/Ni(2 nm) samples both show an average M_S in between thick Ni(15 nm) and CoFeB, demonstrating the influence of ferromagnetic CoFeB on the thin Ni layer, resulting in the entire film stack being ferromagnetic (element specific hysteresis loops shown in Supporting Information S1). Although CoFeB(2 nm)/Ni(2 nm) and Ni(2 nm)/CoFeB(2 nm) films have the same M_S, a closer examination of the SQUID and X-ray magnetic spectroscopy data suggest that the stacking order of the thin films plays a more subtle role in the magnetic properties of the bilayer, such as the coercive field (Supporting Information S1). From these initial results, we infer that parameters such as the film thickness and the stacking order have a significant impact on the magnetic properties and, therefore, on the magnetoelectric coupling in this artificial multiferroic composite. To further explore the effects of these parameters, the magnetic imaging results are shown below.

Main Results In-Operando Magnetic Imaging and Simulation. Following the initial characterization of the magnetic thin films, the magnetoelastic properties of the systems are investigated through voltage-controlled magnetization reorientation experiments in patterned microstructures. The magnetic state of the microsquares is imaged by X-ray magnetic circular dichroism−photoemission electron microscopy (XMCD−PEEM).[22−24] Exploiting the probe depth of approx- imately 5 nm and the elemental sensitivity of X-ray absorption at the Fe and Ni L_3-edges,[22] we are able to separately image the magnetic state in each magnetic layer and compare them with each other (Supporting Media File 1). As shown in Figure 2a, the initial magnetic state observed in both sublayers of the bilayer is the same, proving the presence of strong exchange coupling at the CoFeB/Ni interface. Accordingly, from now on, we present only the XMCD−PEEM images referring to the CoFeB layer for simplicity, unless otherwise noted.

After magnetically initializing the samples by application of an external magnetic field $\mu_0 H_{init}$ = 300 mT, as indicated in Figure 2a, many magnetic squares are observed to be in the Landau magnetic flux-closure states[25,26] (subsequently referred to as the vortex state). However, the initialization yield is smaller than 100%, and in some of the images, microsquares are observed to be in a randomly oriented multidomain state. This could be primarily due to domain wall pinning effects at structural imperfections and also partially due to the inhomogeneous strain at the submicron scale,[7,27] which prevents these squares from relaxing to a vortex state after the magnetic field is removed. In this work, we focus on the behavior of the magnetic

∂

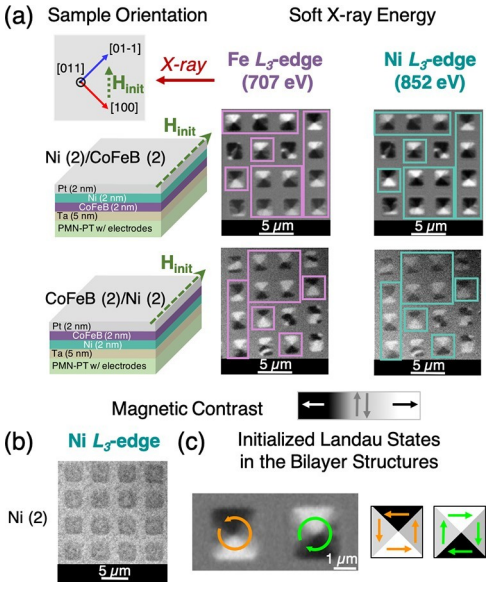

Figure 2. (a) XMCD−PEEM images at Fe and Ni L_3-edges showing the initial magnetic state in bilayer microsquares. Note the similarity in the magnetic state for each device in both the Fe L_3-edge and Ni L_3-edge, evidence of exchange coupling in this system. The purple and turquoise frames indicate where a Landau magnetic flux-closure state is initially observed. The green arrows indicate the initializing magnetic field, $\mu_0 H_{init}$ = 300 mT. The gray scale bar with the arrows describes the contrast levels of magnetic orientation in the PEEM images. (b) Ni L_3- edge XMCD−PEEM of Ni(2 nm) microsquares shows no magnetic contrast as expected for a paramagnetic state. (c) Description of the two types of magnetic vortex states observed in the investigated samples. The schematics of squares in gray scale describe the magnetic configurations in the PEEM images.

squares with an initial vortex state, such as the ones highlighted by purple and turquoise frames in Figure 2a. The reason for investigating these squares is because of the high reliability of electric field-induced reorientation of magnetic vortex states.[27] Schematics of the XMCD−PEEM contrast that indicate vortex states of both chiralities are outlined in Figure 2c.

Further proof of the pivotal role played by the exchange coupling between the Ni and CoFeB layers is shown in Figure 2a,b. The three sets of samples in Figure 2a,b show the magnetic state of three different samples: Ni(2 nm); CoFeB(2 nm)/Ni(2 nm); and Ni(2 nm)/CoFeB(2 nm). While no magnetic contrast is observed in Ni(2 nm) squares, in both Ni/CoFeB samples, the Ni layer shows a magnetic contrast, regardless of the stacking order. The probing depth is sufficient to measure through the entire thickness of the Ni(2 nm) film and shows that Ni(2 nm) alone is not ferromagnetic. Through interfacial exchange coupling with the adjacent CoFeB layer, the Ni layer as well becomes ferromagnetic and the bilayer functions collectively as a single magnetic system, in agreement with the presented SQUID magnetometry measurements in Figure 1b.

To study the electric field-driven magnetic reorientation in the initialized microsquares, we exploit the piezoelectric properties of the PMN−PT substrates. When an electric field is applied along the [011] crystallographic direction of the PMN−PT crystal, a piezostrain is generated along the two main in-plane crystallographic directions,[11,27,28] a compressive strain along the [100] direction, and a tensile strain along the [01−1] direction. This strain is transferred to the magnetic layers deposited on top of the PMN−PT substrate (Figure 1a),

inducing a reorientation of the magnetic moments in the microstructures via the inverse magnetostrictive effect.[7,27,29−31] Furthermore, the direction of the magnetic reorientation is dictated by the sign of the magnetostrictive constant of the specific magnetic material under investigation. We note that Ni has a negative magnetostriction constant, whereas CoFeB has a positive magnetostriction constant.[31] Accordingly, the observa- tion of an electrically driven reorientation of the magnetic state of the microsquares offers an unambiguous way to characterize the magnetoelastic coupling in these systems at the micron scale and to compare the sign and strength of such coupling between different investigated systems.

The initial (E = 0 MV/m) and final (E = 0.8 MV/m) magnetic states of the imaged microsquares are shown in Figure 3 for

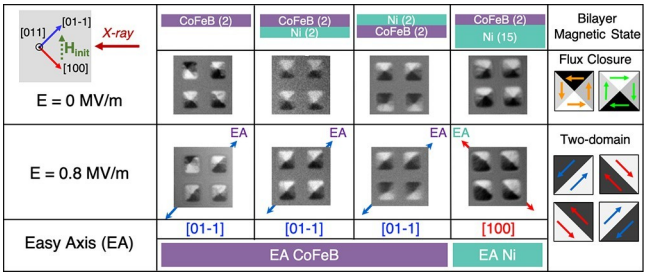

Figure 3. Electric field-controlled magnetic reorientation in 2 μm microsquares from four different Ni/CoFeB bilayer systems. The ratio between the Ni and CoFeB magnetic volumes controls the magneto- electric effect in these multiferroic systems.

samples with different thicknesses of Ni and CoFeB layers. When an electric field is applied, a reorientation of the magnetic moments along one of the principal strain directions is induced, causing the transformation from a magnetic vortex toward a two- domain state. In the sample with a thick Ni layer, we are able to observe a reorientation along the [100] compressive strain direction. In all other samples, the magnetic moments reorient along the [01−1] direction of the substrate. We also observe that the magnetic reorientation effect is weaker in the samples where an equal thickness for the two magnetic layers is chosen [Ni(2 nm); CoFeB(2 nm)] than the magnetic orientation effect in samples with a large difference between the two thicknesses. We can conclude that when the magnetic layer volume is dominated by one of the two materials, the magnetoelastic effect is dictated by that material; However, a more complex effect takes place when the magnetic volumes of Ni and CoFeB are similar.

The behavior described above for nonsymmetric samples can be explained by the magnetostrictive properties of single magnetic materials. As mentioned above, Ni is known to be a negative magnetostrictive material in which the magnetic moments prefer to align along the compressive strain direction, [100] (Table S2).[8,12] In contrast, CoFeB behaves as a positive magnetostrictive material, where the magnetic moments align along the tensile strain direction, [01−1].[10]

The effect of the electric field on magnetic layer reorientation in microsquares of other lateral dimensions (see Supporting Information S3) confirms the same magnetoelastic behavior.

The response observed for the symmetric bilayers calls for a closer investigation. First, the general behavior shows that the CoFeB layer contributes more strongly to the observed magnetoelastic effect than the Ni layer. Second, the effect itself is much weaker than what was observed for the asymmetric samples. Indeed, the magnetic reorientation effect is incomplete,

generating a final state that is in between the vortex state and the two-domain state (see Figure 4 for more details), in the direction

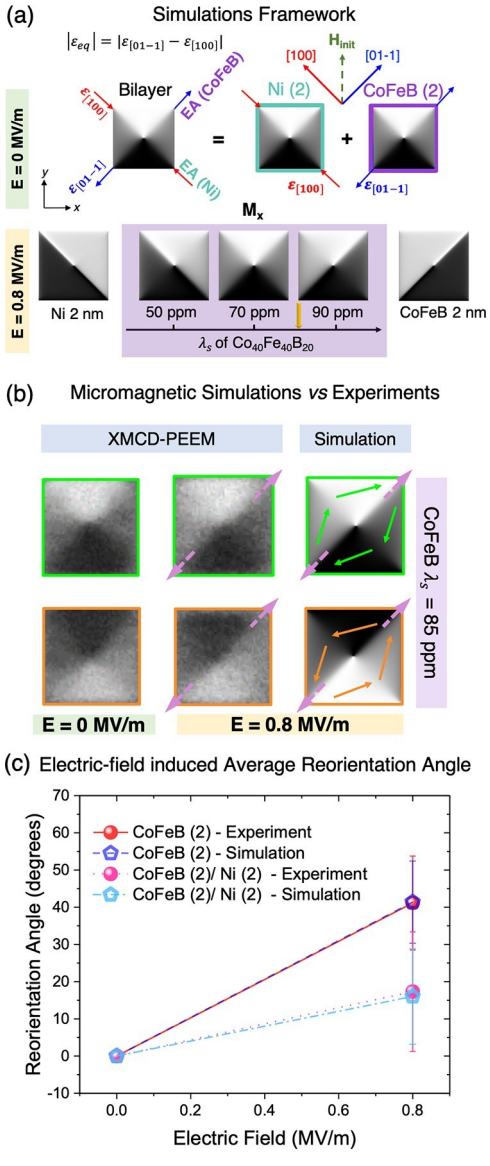

Figure 4. (a) Simulated bilayer micromagnetic system started from a vortex state 0 MV/m (top row) and 0.8 MV/m (bottom row). In the bottom row, the micromagnetic results of single-layer Ni and CoFeB are included on both ends of the spectrum, where the magnetostrictive coefficient of CoFeB is tuned in the range of interest between 50 and 90 ppm. (b) Comparison between micromagnetic outcomes and experimental findings for the CoFeB(2 nm)/Ni(2 nm) system indicate the suitable λ_s value of CoFeB to be 85 ppm. (c) Electric field-induced magnetic moment reorientation angles in CoFeB(2 nm)/PMN−PT and CoFeB(2 nm)/Ni(2 nm)/PMN−PT samples calculated from both experiment and simulation results.

that tends toward the direction of the tensile strain, where CoFeB would have an easy axis. micromagnetic simulations with the goal to reproduce the experimental findings described so far.

Micromagnetic simulations are carried out using the MuMax3 code[32] (see Supporting Information S4 for more details). A 2 μm × 2 μm magnetic Ni/CoFeB square is simulated, where an initial vortex state is nucleated and subsequently modified by the application of a uniaxial anisotropy energy term. Using a phenomenological model to describe the magnetoelastic effect induced in this composite multiferroic system, the electrically controlled strain-induced uniaxial magnetoelastic anisotropy energy density can be evaluated through the following equation[33]

$$U_{\text{m.e.}} = \frac{3}{2}\lambda_s Y\,(\varepsilon_{[01-1]} - \varepsilon_{[100]})\sin^2\theta_{[01-1]} \quad (1)$$

Accordingly, if the observed effect is accounted for by simply summing up the two magnetoelastic effects from the constituent magnetic layers, the interpretation is that the CoFeB layer has a slightly larger magnetoelastic effect than the Ni layer so as to generate the observed magnetic reorientation. However, in order to reach a deeper understanding of our experimental findings, we carry out

where λ_s is the saturation magnetostriction constant for Ni and CoFeB; Y is the average Young's modulus for the two magnetic layers; $\theta_{[01-1]}$ is the angle between the magnetization direction and the tensile strain direction of the piezoelectric, [01−1]; and $\varepsilon_{[01-1]}$ and $\varepsilon_{[100]}$ are the tensile and compressive piezostrains, respectively. From eq 1, it is possible to define a magnetoelastic uniaxial anisotropy factor, $K_{m.e.} = -\frac{3}{2}\lambda_s Y \varepsilon_{eq}$, with $\varepsilon_{eq} = (\varepsilon_{[01-1]} - \varepsilon_{[100]})$, which is a function of the electrically induced piezostrain. The outcomes of micromagnetic simulations are compared to the experimental observations in Figure 4. As can be seen in Figure 4c, the micromagnetic simulations of the CoFeB layer alone and of the CoFeB(2)/Ni(2) bilayer are able to reproduce the experimentally observed behaviors. The simulations for the Ni square reproduce the experimentally observed magnetic reorientation effect[27] in which the initial vortex state completely transforms in a two-domain state with the final magnetization orientation along the compressive strain direction. The same holds for the simulation of the CoFeB square except that the final magnetic state has magnetic moments aligned with the tensile strain direction. The reorientation angle at 0.8 MV/m is calculated to be 41 ± 13° from the experiment and 41 ± 8° from simulation (Figure 4c). The uncertainty of the angles is deviations in the distribution of contrast values in the triangular domains defined for the analysis (explained in detail in Supporting Information S2, Table S1). These values are indeed indicating a full reorientation process because the maximum achievable reorientation angle is 45° in the present experimental geometry. The error bars indicate the average standard deviation of magnetic moment direction distributions in the four magnetic domains forming the initial Landau state. More details on the domain angle analysis are given in Supporting Information S2. After validating our micromagnetic model, we investigate the behavior of CoFeB(2 nm)/Ni(2 nm) squares where we carefully modify the magnetostrictive coefficient of the CoFeB layer. What we learn from this modeling experiment is that in order to reproduce the experimental results (see Supporting Information S4 for more details on parameters), we must assume a magnetostrictive coefficient for CoFeB ($\lambda_s \approx$ 85 ppm) that is more than twice as large, in magnitude, as that of Ni ($\lambda_s = -33$ ppm).[18,33] Indeed, from the experimental data, we can extract a reorientation angle at 0.8 MV/m of 16 ± 16°. Choosing λ_s for CoFeB of 85 ppm, the obtained reorientation angle by micromagnetic simulations is 16 ± 10°, which agrees with the experimental value. Figure 4c shows the quantitative analysis of the average domain rotation angle at 0.8 MV/m when compared to at 0 MV/m for both the single-layer and bilayer samples. The extracted value of λ_s for the CoFeB layer is in general agreement

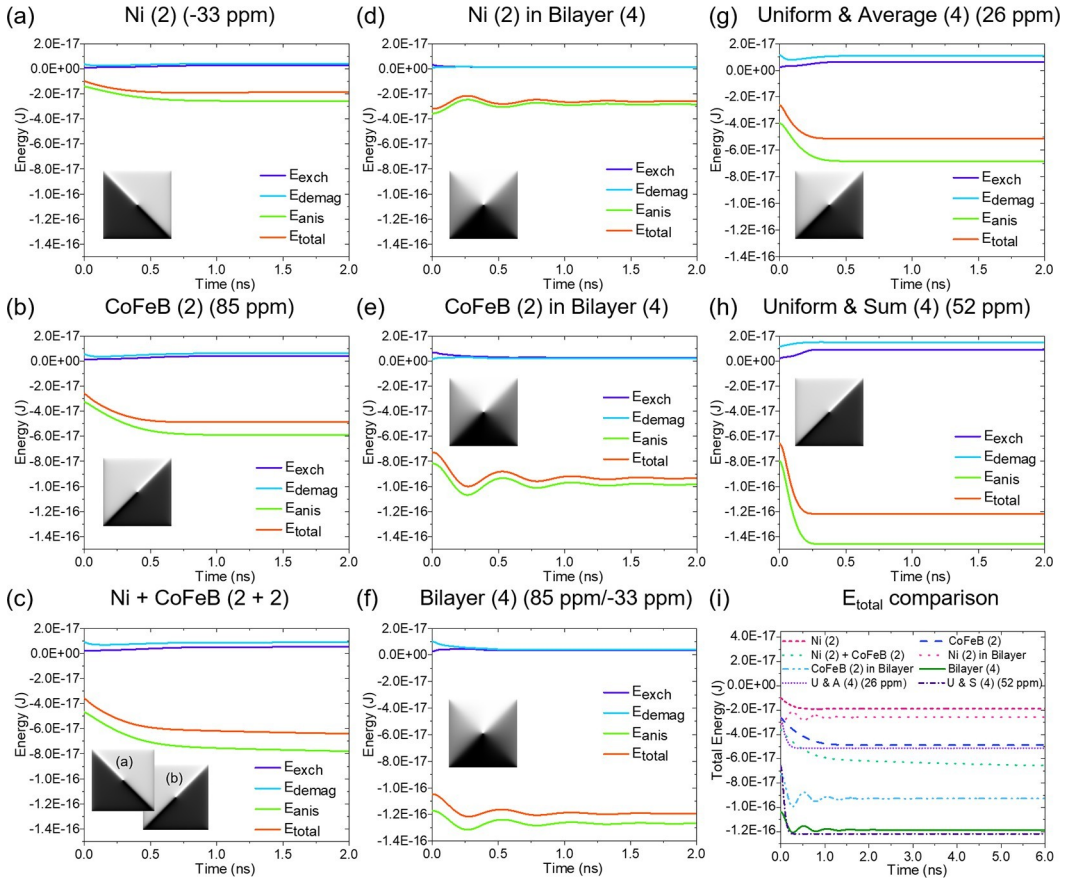

Figure 5. Comparison of energy variations in different 2 μm microsquare systems using micromagnetic simulations starting from the vortex state until reaching an equilibrium state once the equivalent uniaxial anisotropy is applied. We report the variation of exchange energy, demagnetization energy, anisotropy energy, and total energy in (a) single 2 nm thick Ni layer; (b) single 2 nm thick CoFeB layer; (c) system whose energies are the sum of individual energy terms from (a,b); (d) 2 nm thick Ni layer from the CoFeB/Ni bilayer system; (e) 2 nm thick CoFeB layer from the CoFeB/Ni bilayer system; (f) Ni(2 nm)/CoFeB(2 nm) bilayer system; (g) 4 nm thick single layer that takes the averages of the magnetic properties of CoFeB and Ni (M_S = 7.4 × 105 A/m, λ_s = 26 ppm); and (h) 4 nm thick single layer similar to that of (g) but with a λ_s of 52 ppm as the sum of λ_s from CoFeB and Ni. (i) The total energy variation in the eight aforementioned layers and systems. The micromagnetic parameters used for the simulation are reported in Supporting Information S4 Table S2. At the top of each graph, the saturation magnetostriction coefficients (in ppm) used to model the layers and the layer thicknesses are listed in the parentheses. Inset images are the magnetic configurations (m_x) at the final equilibrium states.

with what has been reported previously for $Co_{50}Fe_{50}$, where λ_s was found to be ≈ 70 ppm.[34] $Co_{50}Fe_{50}$ is a very similar material to what is used in this work, where we have equal atomic concentrations of Co and Fe in the $Co_{40}Fe_{40}B_{20}$ composition.

Even if the simulations and the experimental observations seem to agree when reasonable micromagnetic parameters are chosen for our modeling, what is surprising is that the global effect is not simply because of the sum of the two magnetoelastic effects in the two ferromagnetic layers (Figure 5a−c). Indeed, using the phenomenological model described above to calculate the induced magnetoelastic anisotropy contributions from the two layers, we find that

$$K_{m.e.}^{Ni} = -\frac{3}{2}\cdot(33\times10^{-6})\cdot(180\times10^{9})\cdot(1\times10^{-3})/10^{3}$$

and

which allows us to calculate a ratio of $\frac{K_{m.e.}^{Ni}}{K_{m.e.}^{CoFeB}} = 2.29$. Here, the electrically induced strain of 1000 ppm was measured experimentally for PMN−PT that we used from the same growth batch.[12] Accordingly, in order to have the observed incomplete magnetization in terms of the complete bidomain state, the magnetoelastic anisotropy energy density induced in the CoFeB layer needs to be more than twice as large as the one induced in the Ni layer. This is surprising because for an incomplete reorientation, only a slight difference between the two magnetoelastic effects would have been expected, as one would have anticipated from a simple balancing effect approach.

= 8.9 kJ/m^3

This makes it clear that the exchange-coupled magnetoelastic bilayer shows an emergent magnetic behavior that is specific

$$K_{m.e.}^{CoFeB} = \frac{3}{2} \cdot (85 \times 10^{-6}) \cdot (160 \times 10^{9}) \cdot (1 \times 10^{-3})/10^{3} = 20.4 \text{ kJ/m}^3$$

of the hybrid system and not simply the sum of the properties of its constituent. This finding has repercussions on our under- standing of magnetoelastic systems and opens up a new avenue

for the development of novel magnetoelectric materials with

tunable functionalities applicable in multiferroic-based memo- ry,[35] logic,[36] sensors,[37] microwave devices such as antennae,[38] and even in magnetic particles and cell sorting platforms.[28] For

example, in the case of memory applications that uses magnetic tunnel junction (MTJ), the bilayer could serve as the free layer. To further understand how the exchange-coupled bilayer differs from the summation of the two individual layers, the energy terms in different systems before and after applying the strain are reported and compared in Figure 5.

For the single-layer Ni and CoFeB, Figure 5a,b shows the energy variation for exchange energy, demagnetization energy, anisotropy energy, and total energy. Figure 5c reports the sum of the energy terms of the two individual layers Ni(2 nm) and CoFeB(2 nm) in (a) and (b).

On the other hand, Figure 5d−f reports the energetics for the exchange-coupled bilayer system. Figure 5d,e shows the energies in the Ni and CoFeB layer, respectively, whereasFigure 5f reports the sum of each energy term from the two layers. Comparing Figure 5c with Figure 5f, we conclude that because of coupling between the bilayers, the energetics of the bilayer system is not a simple summation of the energy of the two single layers and the effect of additional interactions on the magnetic energy needs to be considered.

In order to reach a deeper understanding of the physics involved in the observed magnetoelastic effect, we simulated ad hoc virtual systems with tailored properties to compare with the actual bilayer system. We have investigated whether a single material with the desired saturation magnetostriction λ_s could replicate such a bilayer system. Here, two virtual systems, called "Uniform & Average" and "Uniform & Sum", are used to estimate the properties of the bilayer. The specifics of those systems are the following: the "Uniform & Average" system consists of a uniform layer of 4 nm in thickness, whose saturation magnetostriction $\lambda_s = \frac{85 + (-33)}{2} = 26$ ppm, damping factor $\alpha = 0.024$, exchange stiffness $A_{ex} = 1.525 \times 10^{-11}$ J/m, and Young's Modulus $Y = 170$ GPa are taken as the averages of those of Ni and CoFeB and whose saturation magnetization $M_S = 7.25 \times 10^5$ A/m is the experimentally measured value (see Supporting Information S4, Table S2 for more details). The "Uniform & Sum" system is identical to "Uniform & Average" apart from its saturation magnetostriction $\lambda_s = 85 + (-33) = 52$ ppm, which is the sum of the saturation magnetostrictions of the two magnetic layers. What we find is that the total magnetic energy at equilibrium of the "average" system in Figure 5g is not the same as the one extracted for the bilayer system reported in Figure 5f; however, the "sum" system (see Figure 5h) is able to reproduce the energetics of the bilayer system even though it still does not produce the same magnetic configuration of the bilayer (same holds for the "average" system).

As a way to identify the importance of exchange coupling at the bilayer interface, which manifests clearly in the calculations of the magnetization dynamics, Figure 5i shows the total energy (of each of the aforementioned simulated systems) as a function of time, starting from the instant in which the initial vortex state begins its relaxation toward the uniaxial magnetoelastic anisotropy direction. Comparison of the Ni and CoFeB layer in the bilayer (Figure 5d,e) with Ni and the CoFeB single layer (Figure 5a,b) indicates the individual layers that become exchange-coupled in the bilayer no longer behave as one when they simulations. Nevertheless, the magnetic configurations in the final state (Figure 5 insets) after applying the strain still differ with both the virtual cases having a two-domain state at equilibrium and the bilayer case still showing four distinct domains in distortion. This result implies that we obtained a synthetic material with tunable properties that is quite different from a single-layer system with material properties given by simply averaging properties of the two layers. The simulation outcomes shine some more light on the complex behavior of the studied system; however, further investigations are needed to reach a full comprehension of the observed phenomenon.

Finally, it is worth noting that in all the subplots in Figure 5, only the coupled bilayer case shows damped oscillations of its energy versus time (Figure 5d,f). Further investigation of the simulation setup indicates that the oscillation arises from the generation of spin waves because of the interface between the two layers. However, the energies at equilibrium (which is the focus of this analysis) are not affected by such transient effects (Supporting Information S4).

For this first demonstration, materials were chosen whose magnetostriction has opposite polarity in order to clearly show the interplay between absolute thickness of each layer, relative thickness of the layers, and the magnetostriction coefficient. Investigation on material combinations that have the same polarity for magnetostriction coefficients is a potential avenue for further investigation. Such studies could give crucial information on how the exchange coupling could further boost the strength of the total magnetoelastic effect achievable in a multiferroic system.

CONCLUSIONS

In summary, the magnetoelastic properties of exchange-coupled Ni/CoFeB magnetic microstructures on top of PMN−PT piezoelectric substrates are investigated as a function of the

stand alone. On the one hand, the summation of the total energies of the Ni and CoFeB single layer at equilibrium is close to the “Uniform & Average” (26 ppm) case which falls into a domain state similar to that of CoFeB. On the other hand, the total energies at equilibrium are very similar between the coupled bilayer and the “Uniform & Sum” (52 ppm) layer

thickness of the two magnetic layers through electric field-driven magnetic reorientation. On the one hand, when the ratio of the two magnetic thicknesses is significantly larger than one, the magnetoelastic properties of the system are dominated by those of the thicker layer. On the other hand, when the layers are of the same thickness, the exchange-coupled microstructures exhibit a more complex behavior, which cannot be described by simply combining the magnetoelastic effects of the two constituent materials. The experimental observations are reproduced by micromagnetic simulations, which support such interpretation. These results demonstrate the richness in magnetoelectric properties offered by exchange-coupled composite multiferroics, where the magnetoelastic effect is governed by the coupling between the two magnetic layers. Furthermore, the tunability of those magnetoelectric properties via magnetic layer composition and stacking order offers a path toward the development of next- generation magnetoelectric systems that could access a richer space of material properties, which can be exploited in the development of novel low-power magnetoelectric devices. This work is expected to motivate more experimental and theoretical studies focused on the magnetoelectric properties of composite multiferroic micro- and nanostructures with exchange-biased magnetic bilayers.

XRD measurements of the thin films; magnetic character- ization of the exchange-coupled multiferroic hetero-structures; quantitative analysis of the magnetic moment direction from PEEM images; magnetic moment reorientation as a function of the field in microstructures of different lateral dimensions; and micromagnetic simulations of magnetic energy variation in single-layer and bilayer systems (PDF)

Animation of the PEEM experiment setup for obtaining the magnetic contrast from the bilayers with the in situ electric field (MP4)

Micromagnetic simulation of the bilayer CoFeB/Ni system with the applied in-plane total strain of 1000 ppm (MP4)

AUTHOR INFORMATION

Corresponding Authors

J. Bokor − *Department of Electrical Engineering and Computer Science, University of California, Berkeley, Berkeley 94720, California, United States; Materials Sciences Division, Lawrence Berkeley National Laboratory, Berkeley 94720, California, United States*; Email: jbokor@berkeley.edu

R. N. Candler − *Department of Electrical and Computer Engineering and Department of Mechanical and Aerospace Engineering, University of California, Los Angeles, Los Angeles 90095, California, United States; California NanoSystems Institute, Los Angeles 90095, California, United States*; Email: rcandler@ucla.edu

Authors

Z. Xiao − *Department of Electrical and Computer Engineering, University of California, Los Angeles, Los Angeles 90095, California, United States; Advanced Light Source, Lawrence Berkeley National Laboratory, Berkeley 94720, California, United States;* orcid.org/0000-0002-7244-8635

R. Lo Conte − *Department of Electrical Engineering and Computer Science, University of California, Berkeley, Berkeley 94720, California, United States;* orcid.org/0000-0002- 5050-9978

M. Goiriena-Goikoetxea − *Department of Electrical Engineering and Computer Science, University of California, Berkeley, Berkeley 94720, California, United States; Department of Electricity and Electronics, University of the Basque Country, Leioa 48940, Spain;* orcid.org/0000-0001-8419-9499

R. V. Chopdekar − *Advanced Light Source, Lawrence Berkeley National Laboratory, Berkeley 94720, California, United States;* orcid.org/0000-0001-6727-6501

C.-H. A. Lambert − *Department of Electrical Engineering and Computer Science, University of California, Berkeley, Berkeley 94720, California, United States*

X. Li − *Department of Electrical and Computer Engineering, University of California, Los Angeles, Los Angeles 90095, California, United States*

A. T. N'Diaye − *Advanced Light Source, Lawrence Berkeley National Laboratory, Berkeley 94720, California, United States*

P. Shafer − *Advanced Light Source, Lawrence Berkeley National Laboratory, Berkeley 94720, California, United States;* orcid.org/0000-0001-9363-2557

S. Tiwari − *Department of Electrical and Computer Engineering, University of California, Los Angeles, Los Angeles 90095, California, United States*

A. Barra − *Department of Mechanical and Aerospace Engineering, University of California, Los Angeles, Los Angeles 90095, California, United States*
A. Chavez − *Department of Mechanical and Aerospace Engineering, University of California, Los Angeles, Los Angeles 90095, California, United States*
K. P. Mohanchandra − *Department of Mechanical and Aerospace Engineering, University of California, Los Angeles, Los Angeles 90095, California, United States*
G. P. Carman − *Department of Mechanical and Aerospace Engineering, University of California, Los Angeles, Los Angeles 90095, California, United States*
K. L. Wang − *Department of Electrical and Computer Engineering, University of California, Los Angeles, Los Angeles 90095, California, United States*
S. Salahuddin − *Department of Electrical Engineering and Computer Science, University of California, Berkeley, Berkeley 94720, California, United States*
E. Arenholz − *Advanced Light Source, Lawrence Berkeley National Laboratory, Berkeley 94720, California, United States*

Complete contact information is available at: https://pubs.acs.org/10.1021/acsami.9b20876

Author Contributions

△Z.X. and R.L.C. contributed equally to this work.

Author Contributions

Z.X. and R.L.C. prepared the manuscript; Z.X. prepared the Supporting Information and designed the figures. R.L.C., Z.X., R.N.C., and J.B. designed the experiments. Z.X., M.G.-G., R.V.C., and R.L.C. carried out the XMCD−PEEM imaging experiments and image analysis. Z.X., X.L., C.-H.A.L., and R.L.C. contributed to sample preparation. Z.X., A.T.N., and P.S. performed soft X-ray spectroscopy experiments. Z.X. carried out SQUID measurements. Z.X., R.V.C., A.B., and A.C. discussed and performed micromagnetics simulations. Z.X. carried out the image processing and quantitative analysis of the results. K.P.M. conducted the XRD measurement given in the Supporting Information. Z.X., R.L.C., R.V.C., M.G.-G., S.T., E.A., and R.N.C. contributed to the interpretation of the results. R.N.C. and J.B. supervised the project. All the authors discussed the results and commented on the manuscript.

Notes

The authors declare no competing financial interest.

ACKNOWLEDGMENTS

We gratefully acknowledge the support from the National Science Foundation (NSF) through the Cooperative Agreement Award EEC-1160504 for Solicitation NSF 11-537 (TANMS) and the NSF Center for Energy Efficient Electronics Science (supporting the sample preparation). The work at the Advanced Light Source at the Lawrence Berkeley National Laboratory (XMCD−PEEM at beamline 11.0.1.1 and X-ray magnetic spectroscopy at beamlines 4.0.2 and 6.3.1) is supported by the Director, Office of Science, Office of Basic Energy Sciences, the U.S. Department of Energy, under contract number DE-AC02- 05CH11231. Z.X. acknowledges the support of the ALS Doctoral Fellowship in Residence (mentored by A.T.N. and E.A.) for part of the work carried out at the Advanced Light Source. M.G.-G. acknowledges the support of the Basque Government for the Postdoctoral Fellowship. We also acknowl- edge the use of the fabrication facility at the Integrated Systems

Nanofabrication Cleanroom of the California NanoSystems Institute.

REFERENCES

(1) Novosad, V.; Otani, Y.; Ohsawa, A.; Kim, S. G.; Fukamichi, K.;
Koike, J.; Maruyama, K.; Kitakami, O.; Shimada, Y. Novel Magneto- strictive Memory Device. *J. Appl. Phys.* 2000, *87*, 6400−6402.

(2) Sasikanth Manipatruni, D. E. N., Ramesh, R., Li, H., Young, I. A., Spin-Orbit Logic with Magnetoelectric Nodes: A Scalable Charge Mediated Nonvolatile Spintronic Logic, 2015. arXiv:1512.05428.

(3) Fiebig, M.; Lottermoser, T.; Meier, D.; Trassin, M. The Evolution of Multiferroics. *Nat. Rev. Mater.* 2016, *1*, 16046.

(4) Lo Conte, R.; Gorchon, J.; Mougin, A.; Lambert, C. H. A.; El- Ghazaly, A.; Scholl, A.; Salahuddin, S.; Bokor, J. Electrically Controlled Switching of the Magnetization State in Multiferroic BaTiO3/CoFe Submicrometer Structures. *Phys. Rev. Mater.* 2018, *2*, No. 091402(R).

(5) Buzzi, M.; Chopdekar, R. V.; Hockel, J. L.; Bur, A.; Wu, T.; Pilet, N.; Warnicke, P.; Carman, G. P.; Heyderman, L. J.; Nolting, F. Single Domain Spin Manipulation by Electric Fields in Strain Coupled Artificial Multiferroic Nanostructures. *Phys. Rev. Lett.* 2013, *111*, 027204.

(6) Sohn, H.; Liang, C.-y.; Nowakowski, M. E.; Hwang, Y.; Han, S.; Bokor, J.; Carman, G. P.; Candler, R. N. Deterministic Multi-step Rotation of Magnetic Single-domain State in Nickel Nanodisks using Multiferroic Magnetoelastic Coupling. *J. Magn. Magn. Mater.* 2017, *439*, 196−202.

(7) Xiao, Z.; Lo Conte, R.; Chen, C.; Liang, C. Y.; Sepulveda, A.; Bokor, J.; Carman, G. P.; Candler, R. N. Bi-directional Coupling in Strain-Mediated Multiferroic Heterostructures with Magnetic Domains and Domain Wall Motion. *Sci. Rep.* 2018, *8*, 5207.

(8) Sohn, H.; Nowakowski, M. E.; Liang, C.-y.; Hockel, J. L.; Wetzlar, K.; Keller, S.; McLellan, B. M.; Marcus, M. A.; Doran, A.; Young, A.; Klaüi, M.; Carman, G. P.; Bokor, J.; Candler, R. N. Electrically Driven Magnetic Domain Wall Rotation in: Multiferroic Heterostructures to Manipulate Suspended On-Chip Magnetic Particles. *ACS Nano* 2015, *9*, 4814−4826.

(9) Hockel, J. L.; Bur, A.; Wu, T.; Wetzlar, K. P.; Carman, G. P. Electric Field Induced Magnetization Rotation in Patterned Ni Ring/ Pb(Mg1/3Nb2/3)O3] ((1-0.32))-[PbTiO3](0.32) Heterostructures. *Appl. Phys. Lett.* 2012, *100*, 022401.

(10) Zhang, S.; Zhao, Y.; Xiao, X.; Wu, Y.; Rizwan, S.; Yang, L.; Li, P.; Wang, J.; Zhu, M.; Zhang, H.; Jin, X.; Han, X. Giant Electrical Modulation of Magnetization in Co40Fe40B20/Pb(Mg1/3Nb2/ 3)0.7Ti0.3O3(011) Heterostructure. *Sci. Rep.* 2014, *4*, 3727.

(11) Zhao, P.; Bao, M.; Bur, A.; Hockel, J. L.; Wong, K.; Mohanchandra, K. P.; Lynch, C. S.; Carman, G. P. Domain Engineered Switchable Strain States in Ferroelectric (011) [Pb(Mg1/3Nb2/ 3)O3](1−x)-[PbTiO3]x(PMN-PT, x≈0.32) Single Crystals. *J. Appl. Phys.* 2011, *109*, 124101.

(12) Xiao, Z.; Mohanchandra, K. P.; Lo Conte, R.; Ty Karaba, C.; Schneider, J. D.; Chavez, A.; Tiwari, S.; Sohn, H.; Nowakowski, M. E.; Scholl, A.; Tolbert, S. H.; Bokor, J.; Carman, G. P.; Candler, R. N. Enhanced Magnetoelectric Coupling in a Composite Multiferroic System via Interposing a Thin Film Polymer. *AIP Adv.* 2018, *8*, 055907.

(13) Lahtinen, T. H. E.; Franke, K. J. A.; van Dijken, S. Electric-field Control of Magnetic Domain Wall Motion and Local Magnetization Reversal. *Sci. Rep.* 2012, *2*, 258.

(14) Chen, J.; Bai, Y.; Nie, C.; Zhao, S. Strong Magnetoelectric Effect of Bi4Ti3O12/Bi5Ti3FeO15 Composite Films. *J. Alloys Compd.* 2016, *663*, 480−486.

(15) Zhao, S.; Wan, J.-g.; Yao, M.; Liu, J.-m.; Song, F.; Wang, G. Flexible Sm−Fe/Polyvinylidene Fluoride Heterostructural Film with Large Magnetoelectric Voltage Output. *Appl. Phys. Lett.* 2010, *97*, 212902.

(16) Bai, Y.; Jiang, N.; Zhao, S. Giant Magnetoelectric Effects in Pseudo 1−3 Heterostructure Films with FeGa Nanocluster-assembled Micron-scale Discs Embedded into Bi5Ti3FeO15 Matrices. *Nanoscale* 2018, *10*, 9816.

(17) Xiao, Z.; Lo Conte, R.; Goiriena, M.; Chopdekar, R. V.; Li, X.; Tiwari, S.; Lambert, C.-H.; Salahuddin, S.; Carman, G. P.; Wang, K.; Bokor, J.; Candler, R. N. Electric-field Controlled Magnetic Reorientation in Exchange Coupled CoFeB/Ni Bilayer Micro- structures. *J. Phys. Conf. Ser.* 2019, *1407*, 012024.

(18) Klokholm, E.; Aboaf, J. The Saturation Magnetostriction of Thin Polycrystalline Films of Iron, Cobalt, and Nickel. *J. Appl. Phys.* 1982, *53*, 2661−2663.

(19) Tsakalakos, T.; Ovid'ko, I. A.; Vasudevan, A. V. *Nanostructures: Synthesis, Functional Properties and Applications*; Springer Science & Business Media, 2003.

(20) Sellmyer, D. J.; Shan, Z. S. Magnetic Hysteresis in Novel Nanostructured Films. In *Magnetic Hysteresis in Novel Magnetic Materials*; Hadjipanayis, G. C., Ed.; Springer: Netherlands, Dordrecht, 1997; pp 419−451.

(21) Neugebauer, C. A. Saturation Magnetization of Nickel Films of Thickness Less Than 100 A. *Phys. Rev.* 1959, *116*, 1441−1446.

(22) Chen, C. T.; Idzerda, Y. U.; Lin, H.-J.; Smith, N. V.; Meigs, G.; Chaban, E.; Ho, G. H.; Pellegrin, E.; Sette, F. Experimental Confirmation of the X-Ray Magnetic Circular-Dichroism Sum-Rules for Iron and Cobalt. *Phys. Rev. Lett.* 1995, *75*, 152−155.

(23) Cheng, X. M.; Keavney, D. J. Studies of Nanomagnetism using Synchrotron-based X-ray Photoemission Electron Microscopy (X- PEEM). *Rep. Prog. Phys.* 2012, *75*, 026501.

(24) Schönhense, G. Imaging of Magnetic Structures by Photo- emission Electron Microscopy. *J. Phys.: Condens. Matter* 1999, *11*, 9517.

(25) Alex Hubert, R. S. *Magnetic Domains: The Analysis of Magnetic Microstructures*; Springer: Berlin, 1998.

(26) Finizio, S.; Kronenberg, A.; Vafaee, M.; Foerster, M.; Litzius, K.; de Lucia, A.; Mentes, T. O.; Aballe, L.; Kruger, B.; Jourdan, M.; Klaui, M. Magnetic Configurations in Nanostructured Co2MnGa Thin Film Elements. *New J. Phys.* 2015, *17*, 083030.

(27) Lo Conte, R.; Xiao, Z.; Chen, C.; Stan, C. V.; Gorchon, J.; El- Ghazaly, A.; Nowakowski, M. E.; Sohn, H.; Pattabi, A.; Scholl, A.; Tamura, N.; Sepulveda, A.; Carman, G. P.; Candler, R. N.; Bokor, J. Influence of Nonuniform Micron-Scale Strain Distributions on the Electrical Reorientation of Magnetic Microstructures in a Composite Multiferroic Heterostructure. *Nano Lett.* 2018, *18*, 1952−1961.

(28) Xiao, Z.; Khojah, R.; Chooljian, M.; Conte, R. L.; Schneider, J. D.; Fitzell, K.; Chopdekar, R. V.; Wang, Y.; Scholl, A.; Chang, J.; Carman, G. P.; Bokor, J.; Di Carlo, D.; Candler, R. N. Cytocompatible Magnetostrictive Microstructures for Nano- and Microparticle Manipulation on Linear Strain Response Piezoelectrics. *Multifunct. Mater.* 2018, *1*, 014004.

(29) Furthmüller, J.; Faẗnle, M.; Herzer, G. Theory of Magneto-striction in Amorphous and Polycrystalline Ferromagnets. *J. Magn. Magn. Mater.* 1987, *69*, 79−88.

(30) Lee, E. W. Magnetostriction and Magnetomechanical Effects. *Rep. Prog. Phys.* 1955, *18*, 184−229.

(31) Bichurin, M. I.; Petrov, V. M.; Srinivasan, G. Theory of Low- frequency Magnetoelectric Coupling in Magnetostrictive-Piezoelectric Bilayers. *Phys. Rev. B: Condens. Matter Mater. Phys.* 2003, *68*, 054402.

(32) Vansteenkiste, A.; Leliaert, J.; Dvornik, M.; Helsen, M.; Garcia- Sanchez, F.; Van Waeyenberge, B. The Design and Verification of MuMax3. *AIP Adv.* 2014, *4*, 107133.

(33) O'Handley, R. C. *Modern Magnetic Materials*; John Wiley & Sons, Inc. Scientific, Technical, and Medical Division: USA, 2000.

(34) Hunter, D.; Osborn, W.; Wang, K.; Kazantseva, N.; Hattrick- Simpers, J.; Suchoski, R.; Takahashi, R.; Young, M. L.; Mehta, A.; Bendersky, L. A.; Lofland, S. E.; Wuttig, M.; Takeuchi, I. Giant Magnetostriction in Annealed Co(1-x)Fe(x) thin-films. *Nat. Commun.* 2011, *2*, 518.

(35) Wang, Q.; Li, X.; Liang, C.-Y.; Barra, A.; Domann, J.; Lynch, C.; Sepulveda, A.; Carman, G. P. Strain-mediated 180° Switching in CoFeB and Terfenol-D Nanodots with Perpendicular Magnetic Anisotropy. *Appl. Phys. Lett.* 2017, *110*, 102903.

(36) D'Souza, N.; Atulasimha, J.; Bandyopadhyay, S. Four-state Nanomagnetic Logic using Multiferroics. *J. Phys. D: Appl. Phys.* 2011, *44*, 265001.

(37) Multiferroics March On. *Nat. Mater.* 2019, *18*, 187. DOI: 10.1038/s41563-019-0310-y
(38)Yao, Z.; Wang, Y. E.; Keller, S.; Carman, G. P. Bulk Acoustic Wave-Mediated Multiferroic Antennas: Architecture and Performance Bound. *IEEE Trans. Antennas Propag.* 2015, *63*, 3335−3344.